ARTICLE NO. 78-10R

J80-031

Implicit Finite-Difference Simulations of Three-Dimensional Compressible Flow

20005
20019

Thomas H. Pulliam* and Joseph L. Steger*
NASA Ames Research Center, Moffett Field, Calif.

An implicit finite-difference procedure for unsteady three-dimensional flow capable of handling arbitrary geometry through the use of general coordinate transformations is described. Viscous effects are optionally incorporated with a "thin-layer" approximation of the Navier-Stokes equations. An implicit approximate factorization technique is employed so that the small grid sizes required for spatial accuracy and viscous resolution do not impose stringent stability limitations. Results obtained from the program include transonic inviscid or viscous solutions about simple body configurations. Comparisons with existing theories and experiments are made. Numerical accuracy and the effect of three-dimensional coordinate singularities are also discussed.

I. Introduction

A COMBINATION of general curvilinear coordinate transformations, well-ordered grids, and an implicit algorithm is used here to construct a versatile three-dimensional program for unsteady or steady inviscid and viscous compressible flow. While we generally look to the future for computers with more speed and storage, the computers of today can calculate meaningful numerical solutions about relatively simple three-dimensional body shapes. The need to progress to three dimensions on current computers is twofold: 1) to demonstrate to the user community that complex geometries and body motions will not present any great difficulty to routine solution given computers one or two orders of magnitude more powerful than what is available today, and 2) to provide simple, three-dimensional flowfield solutions to test current and future turbulence models.

The three-dimensional program described herein demonstrates one technique that can be applied to solve flowfields about simple (present application) and complicated (future applications) aerodynamic shapes. General transformations[1-4] valid for any body configuration or grid system are used. An implicit approximate factorization method[5-8] is chosen chiefly for its unconditional linear stability property, as well as for its compatibility with the vectorized computer processors[9] that seem to be the trend of the future. The overall algorithm constructed here is both simple and flexible; its extension to other problems and computers should be reasonably straightforward.

In Sec. II the equations, generalized transformations, and boundary conditions are presented, along with a "thin-layer" viscous approximation. The numerical algorithm is described in Sec. III, while the geometry and grid systems are discussed in Sec. IV. Results and their discussion appear in Sec. V.

Presented as Paper 78-10 at the AIAA 16th Aerospace Sciences Meeting, Huntsville, Ala., Jan. 16-18, 1978; submitted June 5, 1978; revision received Aug. 6, 1979.

Index categories: Computational Methods; Viscous Nonboundary-Layer Flows.

*Research Scientist; presently with Flow Simulations Inc., Sunnyvale, Calif. Member AIAA.

II. Transformed Equations

To enhance numerical accuracy and efficiency, coordinate mappings of the governing equations are employed which bring all body surfaces onto coordinate surfaces, and cluster grid points in flowfield regions where the dependent variables are expected to undergo rapid changes of gradient. In the transformed plane, uniform discretization formulas and well-ordered interior grid point solution algorithms can be used. The equations can also be written in strong conservation law form for shock-capturing purposes and to avoid possible weak instability from source terms. These considerations led to the general transformed equations with the additional simplifications that are discussed in this section. Related work using comparable transforms in flowfield applications can be found in Refs. 10-15.

A. Equations in Nondimensional Form

If inertial Cartesian velocity components are retained as dependent variables, the three-dimensional, unsteady Navier-Stokes equations can be transformed to the arbitrary curvilinear space ξ,η,ζ,τ shown in Fig. 1a, while retaining strong conservation law form (see Refs. 1-4). The resulting transformed equations are not much more complicated than the original Cartesian set, and can be written in nondimensional form as

$$\partial_\tau \hat{q} + \partial_\xi (\hat{E} - \hat{E}_v) + \partial_\eta (\hat{F} - \hat{F}_v) + \partial_\zeta (\hat{G} - \hat{G}_v) = 0 \qquad (1)$$

where

$$\hat{q} = J^{-1} \begin{bmatrix} \rho \\ \rho u \\ \rho v \\ \rho w \\ e \end{bmatrix} \quad \hat{E} = J^{-1} \begin{bmatrix} \rho U \\ \rho u U + \xi_x p \\ \rho v U + \xi_y p \\ \rho w U + \xi_z p \\ (e+p)U - \xi_t p \end{bmatrix}$$

$$\hat{F} = J^{-1} \begin{bmatrix} \rho V \\ \rho u V + \eta_x p \\ \rho v V + \eta_y p \\ \rho w V + \eta_z p \\ (e+p)V - \eta_t p \end{bmatrix} \quad \hat{G} = J^{-1} \begin{bmatrix} \rho W \\ \rho u W + \zeta_x p \\ \rho v W + \zeta_y p \\ \rho w W + \zeta_z p \\ (e+p)W - \zeta_t p \end{bmatrix} \qquad (2)$$

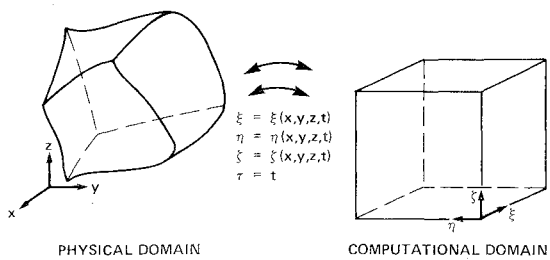

a)

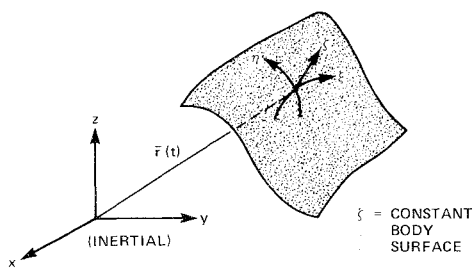

b)

Fig. 1 Transformations and body coordinate.

and

$$U=\xi_t+\xi_x u+\xi_y v+\xi_z w$$

$$V=\eta_t+\eta_x u+\eta_y v+\eta_z w$$

$$W=\zeta_t+\zeta_x u+\zeta_y v+\zeta_z w \tag{3}$$

where U, V, and W are contravariant velocities written without metric normalization (see, for instance, Ref. 16). (Note that other suggestive forms of the equations can be written; for example,

$$U=\xi_x(u-x_\tau)+\xi_y(v-y_\tau)+\xi_z(w-z_\tau)$$

where $(u-x_\tau)$, etc. are relative Cartesian velocity components.)

The viscous flux terms are given by

$$\hat{E}_v=J^{-1}\begin{bmatrix}0\\ \xi_x\tau_{xx}+\xi_y\tau_{xy}+\xi_z\tau_{xz}\\ \xi_x\tau_{yx}+\xi_y\tau_{yy}+\xi_z\tau_{yz}\\ \xi_x\tau_{zx}+\xi_y\tau_{zy}+\xi_z\tau_{zz}\\ \xi_x\beta_x+\xi_y\beta_y+\xi_z\beta_z\end{bmatrix}$$

$$\hat{F}_v=J^{-1}\begin{bmatrix}0\\ \eta_x\tau_{xx}+\eta_y\tau_{xy}+\eta_z\tau_{xz}\\ \eta_x\tau_{yx}+\eta_y\tau_{yy}+\eta_z\tau_{yz}\\ \eta_x\tau_{zx}+\eta_y\tau_{zy}+\eta_z\tau_{zz}\\ \eta_x\beta_x+\eta_y\beta_y+\eta_z\beta_z\end{bmatrix} \tag{4}$$

$$\hat{G}_v=J^{-1}\begin{bmatrix}0\\ \zeta_x\tau_{xx}+\zeta_y\tau_{xy}+\zeta_z\tau_{xz}\\ \zeta_x\tau_{yx}+\zeta_y\tau_{yy}+\zeta_z\tau_{yz}\\ \zeta_x\tau_{zx}+\zeta_y\tau_{zy}+\zeta_z\tau_{zz}\\ \zeta_x\beta_x+\zeta_y\beta_y+\zeta_z\beta_z\end{bmatrix}$$

and

$$\tau_{xx}=\lambda(u_x+v_y+w_z)+2\mu u_x$$

$$\tau_{xy}=\tau_{yx}=\mu(u_y+v_x)$$

$$\tau_{xz}=\tau_{zx}=\mu(u_z+w_x)$$

$$\tau_{yy}=\lambda(u_x+v_y+w_z)+2\mu v_y$$

$$\tau_{yz}=\tau_{zy}=\mu(v_z+w_y)$$

$$\tau_{zz}=\lambda(u_x+v_y+w_z)+2\mu w_z$$

$$\beta_x=\gamma\kappa Pr^{-1}\partial_x e_I+u\tau_{xx}+v\tau_{xy}+w\tau_{xz}$$

$$\beta_y=\gamma\kappa Pr^{-1}\partial_y e_I+u\tau_{yx}+v\tau_{yy}+w\tau_{yz}$$

$$\beta_z=\gamma\kappa Pr^{-1}\partial_z e_I+u\tau_{zx}+v\tau_{zy}+w\tau_{zz}$$

$$e_I=e\rho^{-1}-0.5(u^2+v^2+w^2) \tag{5}$$

Here it is understood that the Cartesian derivatives are to be expanded in ξ,η,ζ space via chain-rule relations such as

$$u_x=\xi_x u_\xi+\eta_x u_\eta+\zeta_x u_\zeta$$

The Cartesian velocity components u, v, w are nondimensionalized with respect to a_∞ (the freestream speed of sound), density ρ is referenced to ρ_∞; and total energy e to $\rho_\infty a_\infty^2$. Pressure is defined as

$$p=(\gamma-1)[e-0.5\rho(u^2+v^2+w^2)] \tag{6}$$

and throughout γ is the ratio of specific heats. Also, κ is the coefficient of thermal conductivity, μ is the dynamic viscosity, while λ from the Stokes' hypothesis is $-\frac{2}{3}\mu$. The Reynolds number is Re and the Prandtl number is Pr.

Finally, the metric terms are obtained from chain-rule expansion of x_ξ, y_ξ, etc., and solved for ξ_x, ξ_y, etc., to give

$$\xi_x=J(y_\eta z_\zeta-y_\zeta z_\eta) \qquad \eta_x=J(z_\xi y_\zeta-y_\xi z_\zeta)$$

$$\xi_y=J(z_\eta x_\zeta-x_\eta z_\zeta) \qquad \eta_y=J(x_\xi z_\zeta-x_\zeta z_\xi)$$

$$\xi_z=J(x_\eta y_\zeta-y_\eta x_\zeta) \qquad \eta_z=J(y_\xi x_\zeta-x_\xi y_\zeta)$$

$$\zeta_x=J(y_\xi z_\eta-z_\xi y_\eta) \qquad \xi_t=-x_\tau\xi_x-y_\tau\xi_y-z_\tau\xi_z$$

$$\zeta_y=J(x_\eta z_\xi-x_\xi z_\eta) \qquad \eta_t=-x_\tau\eta_x-y_\tau\eta_y-z_\tau\eta_z$$

$$\zeta_z=J(x_\xi y_\eta-y_\xi x_\eta) \qquad \zeta_t=-x_\tau\zeta_x-y_\tau\zeta_y-z_\tau\zeta_z \tag{7}$$

and

$$J^{-1}=x_\xi y_\eta z_\zeta+x_\zeta y_\xi z_\eta+x_\eta y_\zeta z_\xi-x_\xi y_\zeta z_\eta-x_\eta y_\xi z_\zeta-x_\zeta y_\eta z_\xi$$

B. Thin-Layer Approximation

In high Reynolds number flows, one usually has only enough grid points to resolve viscous terms in a thin layer near rigid boundaries. Typically, grid lines are clustered near a body and resolution along the body is similar to what is needed in inviscid flow. Even though the full Navier-Stokes equations may be programmed, viscous derivatives along the body are not resolved in general unless the streamwise and circumferential grid spacings are sufficiently small, in many cases of $0(Re^{-\frac{1}{2}})$ based on the effective viscosity coefficient. Consequently, a thin-layer approximation is used; all viscous derivatives in the ξ and η direction (along the body) are neglected, while terms in ζ are retained and the body surface is mapped onto $\zeta=$ const (see Figs. 1b and 2). Equation (1) thus

simplifies to

$$\partial_\tau \hat{q} + \partial_\xi \hat{E} + \partial_\eta \hat{F} + \partial_\zeta \hat{G} = Re^{-1} \partial_\zeta \hat{S} \tag{8}$$

where

$$\hat{S} = J^{-1} \begin{bmatrix} 0 \\ \mu(\zeta_x^2 + \zeta_y^2 + \zeta_z^2) u_\zeta + (\mu/3)(\zeta_x u_\zeta + \zeta_y v_\zeta + \zeta_z w_\zeta)\zeta_x \\ \mu(\zeta_x^2 + \zeta_y^2 + \zeta_z^2) v_\zeta + (\mu/3)(\zeta_x u_\zeta + \zeta_y v_\zeta + \zeta_z w_\zeta)\zeta_y \\ \mu(\zeta_x^2 + \zeta_y^2 + \zeta_z^2) w_\zeta + (\mu/3)(\zeta_x u_\zeta + \zeta_y v_\zeta + \zeta_z w_\zeta)\zeta_z \\ \{(\zeta_x^2 + \zeta_y^2 + \zeta_z^2)[0.5\mu(u^2 + v^2 + w^2)_\zeta \\ + \kappa Pr^{-1}(\gamma - 1)^{-1}(a^2)_\zeta] + (\mu/3)(\zeta_x u + \zeta_y v + \zeta_z w) \\ \times(\zeta_x u_\zeta + \zeta_y v_\zeta + \zeta_z w_\zeta)\} \end{bmatrix} \tag{9}$$

In the thin-layer model, a boundary-layer-like coordinate is adopted and the viscous terms that are dropped in boundary-layer theory are eliminated. It should be stressed that the thin-layer approximation is valid only for high Reynolds number flows and that very large turbulent viscosity coefficients could conceivably invalidate the model.

As noted earlier, the thin-layer model requires a boundary-layer-type coordinate system. To use this model near the intersection of a vertical and horizontal wall, for example, would require treating both walls as a single continuous surface which is mapped into the same $\zeta = \text{const}$ plane. If these conditions are violated, the neglected viscous terms should and can be added to the present numerical procedure (Refs. 6, 8, 22, and 23).

The concept of a thin-layer viscous model has been employed by others, notably, Cheng,[17] Rubin and Lin,[18] Lubard and Helliwell,[19] McDonald and Briley,[20] and Davis,[21] within the framework of the parabolized Navier-Stokes equations or the thin shock-layer approximations. Because these are sometimes space-marching procedures, we avoid this terminology here; that is, "parabolized Navier-Stokes." In space-marching methods, additional restrictions must be placed on the streamwise (i.e., ξ) convection terms and their boundary conditions, whereas, such restrictions are not made here. Consequently, unlike the space-marching procedures, the present treatment of the unsteady equations, Eq. (8), is valid for streamwise as well as crossflow separation and does not require additional approximation in subsonic flow regions.

C. Surface Boundary Conditions

The tangency condition along the surface $\zeta(x,y,z,t) = \text{const}$ for inviscid flow is that $W = 0$ and is used in

$$\begin{bmatrix} u \\ v \\ w \end{bmatrix} = J^{-1} \begin{bmatrix} (\eta_y \zeta_z - \eta_z \zeta_y) & -(\xi_y \zeta_z - \xi_z \zeta_y) & (\xi_y \eta_z - \eta_y \xi_z) \\ -(\eta_x \zeta_z - \eta_z \zeta_x) & (\xi_x \zeta_z - \xi_z \zeta_x) & -(\xi_x \eta_z - \xi_z \eta_x) \\ (\eta_x \zeta_y - \eta_y \zeta_x) & -(\xi_x \zeta_y - \xi_y \zeta_x) & (\xi_x \eta_y - \xi_y \eta_x) \end{bmatrix} \begin{bmatrix} U - \xi_t \\ V - \eta_t \\ W - \zeta_t \end{bmatrix} \tag{10}$$

to obtain u, v, and w. For viscous flow, $U = V = 0$ are enforced in Eq. (10) as well.

A relation for pressure along the body surface is obtained from a normal momentum relation (found by combining the three transformed momentum equations)

$$p_n(\zeta_x^2 + \zeta_y^2 + \zeta_z^2)^{1/2} = (\xi_x \zeta_x + \xi_y \zeta_y + \xi_z \zeta_z) p_\xi + (\eta_x \zeta_x + \eta_y \zeta_y + \eta_z \zeta_z) p_\eta + (\zeta_x^2 + \zeta_y^2 + \zeta_z^2) p_\zeta$$
$$= \rho[\partial_\tau \zeta_t + u \partial_\tau \zeta_x + v \partial_\tau \zeta_y + w \partial_\tau \zeta_z] - \rho U(\zeta_x u_\xi + \zeta_y v_\xi + \zeta_z w_\xi) - \rho V(\zeta_x u_\eta + \zeta_y v_\eta + \zeta_z w_\eta) \tag{11}$$

where n is the normal direction to the body surface. For viscous flows, the same relation is used with $U = V = 0$. All of the preceding boundary conditions are valid for steady or unsteady body motion.

III. Numerical Method

The finite-difference scheme is the implicit approximate factorization algorithm used in the delta form described by Beam and Warming.[7,8] An implicit method was chosen to avoid restrictive stability conditions which occur when small grid spacing is used. Highly refined grids are needed to obtain spatial accuracy and resolution of large gradients such as occur in calculating viscous effects. Small grid sizes may also occur because nonoptimal mappings overly concentrate points in a given region. Implicit methods are useful in avoiding stiffness in problems in which the solution is forced. In such cases, time steps that are large compared to those demanded by an explicit stability limit can often be taken without degradation of accuracy.

The basic algorithm is first- or second-order accurate in time and is noniterative. The equations are factored (spatially split), which reduces the solution process to three one-dimensional problems at a given time level. Central-difference operators are employed and the algorithm produces block tridiagonal systems for each space coordinate. The stability and accuracy of the numerical algorithm are described in detail by Warming and Beam.[22] Linear analysis of the numerical scheme shows that it is unconditionally stable, although in actual practice, the nonlinear equations are subject to a time-step limitation. The limitation, though, is usually much less stringent than what is found for conventional explicit schemes. The numerical scheme can be first- or second-order accurate in time (for the steady-state cases presented here, first-order accuracy is employed), with second- or fourth-order accuracy in space.

A. Approximate Factorizations and Linearizations

The finite-difference algorithm applied to Eq. (8) results in the following approximate factorization

$$(I + h\delta_\xi \hat{A}^n - \epsilon_I J^{-1} \nabla_\xi \Delta_\xi J)(I + h\delta_\eta \hat{B}^n - \epsilon_I J^{-1} \nabla_\eta \Delta_\eta J)$$
$$(I + h\delta_\zeta \hat{C}^n - hRe^{-1} \delta_\zeta J^{-1} \hat{M}^n J - \epsilon_I J^{-1} \nabla_\zeta \Delta_\zeta J)(\hat{q}^{n+1} - \hat{q}^n)$$
$$\delta_\zeta = -\Delta t(\delta_\xi \hat{E}^n + \delta_\eta \hat{F}^n + \delta_\zeta \hat{G}^n - Re^{-1} \delta_\zeta \hat{S}^n) - \epsilon_E J^{-1}[(\nabla_\xi \Delta_\xi)^2 + (\nabla_\eta \Delta_\eta)^2 + (\nabla_\zeta \Delta_\zeta)^2] J \hat{q}^n \tag{12}$$

where the δ's are central-difference operators, and Δ and ∇ are forward and backward-difference operators, e.g., $\Delta_\zeta q = q(\xi,\eta,\zeta+\Delta\zeta) - q(\xi,\eta,\zeta)$. Indices denoting spatial location are suppressed for convenience and $h = \Delta t$ corresponds to Euler implicit first-order and $h = \Delta t/2$ to trapezoidal second-order time accuracy.

The Jacobian matrices $\hat{A}^n$, $\hat{B}^n$, and $\hat{C}^n$ are obtained in the time linearization of $\hat{E}^n$, $\hat{F}^n$, and $\hat{G}^n$ and can be written as

$$\hat{A},\hat{B},\text{ or }\hat{C}=\begin{bmatrix} K_0 & K_1 & K_2 & K_3 & 0 \\ K_1\phi^2-u\theta & K_0+\theta-K_1(\gamma-2)u & K_2u-(\gamma-1)K_1v & K_3u-(\gamma-1)K_1w & K_1(\gamma-1) \\ K_2\phi^2-v\theta & K_1v-K_2(\gamma-1)u & K_0+\theta-K_2(\gamma-2)v & K_3v-(\gamma-1)K_2w & K_2(\gamma-1) \\ K_3\phi^2-w\theta & K_1w-K_3(\gamma-1)u & K_2w-K_3(\gamma-1)v & K_0+\theta-K_3(\gamma-2)w & K_3(\gamma-1) \\ \theta[2\phi^2-\gamma(e/\rho)] & \{K_1[\gamma(e/\rho)-\phi^2] & \{K_2[\gamma(e/\rho)-\phi^2] & \{K_3[\gamma(e/\rho)-\phi^2] & K_0+\gamma\theta \\ & -(\gamma-1)u\theta\} & -(\gamma-1)v\theta\} & -(\gamma-1)w\theta\} & \end{bmatrix} \tag{13}$$

where

$$\phi^2=0.5(\gamma-1)(u^2+v^2+w^2)$$

$$\theta=K_1u+K_2v+K_3w$$

and, for example, to obtain $\hat{A}$,

$$K_0=\xi_t,\quad K_1=\xi_x,\quad K_2=\xi_y,\quad K_3=\xi_z$$

The viscous vector $\hat{S}^{n+1}$ is linearized by Taylor series as in Ref. 13, producing the coefficient matrix

$$\hat{M}^n=\begin{bmatrix} 0 & 0 & 0 & 0 & 0 \\ m_{21} & \alpha_1\delta_\zeta(\rho^{-1}) & \alpha_2\delta_\zeta(\rho^{-1}) & \alpha_3\delta_\zeta(\rho^{-1}) & 0 \\ m_{31} & \alpha_2\delta_\zeta(\rho^{-1}) & \alpha_4\delta_\zeta(\rho^{-1}) & \alpha_5\delta_\zeta(\rho^{-1}) & 0 \\ m_{41} & \alpha_3\delta_\zeta(\rho^{-1}) & \alpha_5\delta_\zeta(\rho^{-1}) & \alpha_6\delta_\zeta(\rho^{-1}) & 0 \\ m_{51} & m_{52} & m_{53} & m_{54} & \alpha_0\delta_\zeta(\rho^{-1}) \end{bmatrix} \tag{14}$$

with

$$m_{21}=\alpha_1\delta_\zeta(-u/\rho)+\alpha_2\delta_\zeta(-v/\rho)+\alpha_3\delta_\zeta(-w/\rho)$$

$$m_{31}=\alpha_2\delta_\zeta(-u/\rho)+\alpha_4\delta_\zeta(-v/\rho)+\alpha_5\delta_\zeta(-w/\rho)$$

$$m_{41}=\alpha_3\delta_\zeta(-u/\rho)+\alpha_5\delta_\zeta(-v/\rho)+\alpha_6\delta_\zeta(-w/\rho)$$

$$m_{51}=\alpha_1\delta_\zeta(-u^2/\rho)+\alpha_2\delta_\zeta(-2uv/\rho)+\alpha_3\delta_\zeta(-2uw/\rho)$$
$$+\alpha_4\delta_\zeta(-v^2/\rho)+\alpha_6\delta_\zeta(-w^2/\rho)+\alpha_5\delta_\zeta(-2vw/\rho)$$
$$+\alpha_0\delta_\zeta(-e/\rho^2)+\alpha_0\delta_\zeta[(u^2+v^2+w^2)/\rho]$$

$$m_{52}=-m_{21}-\alpha_0\delta_\zeta(u/\rho),\quad m_{53}=-m_{31}-\alpha_0\delta_\zeta(v/\rho)$$

$$m_{54}=-m_{41}-\alpha_0\delta_\zeta(w/\rho)$$

$$\alpha_0=\gamma\kappa Pr^{-1}(\zeta_x^2+\zeta_y^2+\zeta_z^2),\quad \alpha_1=\mu[(4/3)\zeta_x^2+\zeta_y^2+\zeta_z^2]$$

$$\alpha_2=(\mu/3)\zeta_x\zeta_y,\quad \alpha_3=(\mu/3)\zeta_x\zeta_z$$

$$\alpha_4=\mu[\zeta_x^2+(4/3)\zeta_y^2+\zeta_z^2],\quad \alpha_5=(\mu/3)\zeta_y\zeta_z$$

$$\alpha_6=\mu[\zeta_x^2+\zeta_y^2+(4/3)\zeta_z^2] \tag{15}$$

B. Explicit and Implicit Numerical Dissipation

Fourth-order dissipation terms such as $\epsilon_E J^{-1}(\nabla_\xi\Delta_\xi)^2J\hat{q}$ in Eq. (12) are added explicitly to the equations to damp high-frequency growth and thus serve to control nonlinear instability. Linear stability analysis shows that the coefficient ϵ_E must be less than 1/24. The addition of the implicit second-difference terms operating on $(\hat{q}^{n+1}-\hat{q}^n)$ with coefficient ϵ_I extends the linear stability bound of the fourth-order terms. Although linear stability theory based on periodic boundary conditions shows that the stability-bound ϵ_E is again limited, unpublished analysis by Jean-Antoine Desideri of Iowa State University suggests that unconditional stability can be obtained for fixed boundary conditions if ϵ_I is sufficiently large, and numerical experiments confirm this. The present procedure is to set $\epsilon_E=\Delta t$ and $\epsilon_I=2\epsilon_E$, which results in a consistent definition of ϵ_E; as the time step is increased, the amount of artificial dissipation added relative to the spatial derivatives of convection and diffusion remains constant. The implicit smoothing term adds an error $0(\Delta t\Delta x^2q_{xxt})$.

C. Second- and Fourth-Order Accuracy of Convection Terms

Generally, we have used second-order, central-difference operators for convection and diffusion derivatives. In three dimensions we are forced into somewhat coarse grids due to limitations of computer storage. For improved accuracy, it is desirable to use fourth-order accurate convective differencing, especially in high Reynolds number viscous flow in which it can be difficult to keep the convection truncation error from exceeding the magnitude of the viscous terms themselves. One possibility is to use fourth-order Pade differencing for convection terms and second-order Pade differencing for diffusion terms.[23] If the time variation of the solution is small, however, the same effect is obtained by remaining first-order accurate in time and by using five-point, fourth-order accurate central differencing for the right-hand-side convection terms in Eq. (12). Because fourth-order differences are applied only as an explicit operation, little additional work is necessary. One can show that for Euler implicit time differencing, the altered algorithm remains unconditionally stable; it is, however, unconditionally unstable for trapezoidal differencing.

D. Differencing the Metrics to Maintain the Freestream

The metric terms ξ_x, η_x, etc., are formed from x,y,z data using second-order, central-difference approximations of x_ξ, x_η, etc. in Eq. (7). In three dimensions, a freestream error can be introduced, unless, for example, this differencing is done with special weighted averages (see Ref. 24). However,

calculations have been made on smoothly varying grids without attempting to maintain freestream; compared with results in which freestream is maintained using the averaging procedure, there was no discernible difference in the solution on the body.

Perfect maintenance of the freestream can also be achieved by simply subtracting the freestream fluxes from the governing equations; that is,

$$\partial_\tau \hat{q} + \partial_\xi (\hat{E} - \hat{E}_\infty) + \partial_\eta (\hat{F} - \hat{F}_\infty) + \partial_\zeta (\hat{G} - \hat{G}_\infty) = Re^{-1} \partial_\zeta \hat{S} \tag{16}$$

where the error in the viscous term is neglected since it will be small for high Reynolds number flow. This procedure is adopted for all subsequent calculations.

E. Implementing Boundary Conditions

Unknown values of $\hat{q}$ on the boundaries are updated explicitly. Thus, $\Delta\hat{q}$ is set to zero at the boundaries leading to a first-order error in time. One intuitively expects implicit boundary conditions to be more stable than explicit ones. With our treatment of boundary conditions, however, this has not been our experience, at least for the various implicit boundary schemes that have been successfully implemented so far in two dimensions. In any event, explicit treatment of the boundaries leads to a far more simple and flexible scheme, where boundary conditions become a modular element that can be put in or pulled out of a computer program without disturbing the implicit algorithm.

For inviscid flows, values of ρ, U, and V along the body surface are found by linear extrapolation from above, while in viscous cases ρ is extrapolated and $U = V = 0$. In either case, $W = 0$ and values of u, v, and w are obtained from Eq. (10).

Surface pressure is obtained by integrating Eq. (11). In Eq. (11) the right-hand side is known from the previous extrapolation process, and the basic approximate factorization algorithm is applied along the body using backward differencing in ζ and central differences in ξ and η. Scalar tridiagonals are thus inverted in the ξ and η directions. At the farfield boundaries, freestream values are specified except on the downstream boundary. There, a simple first-order extrapolation is used for $M_\infty \geq 1$, while extrapolation and the condition that pressure is fixed at p_∞ is used for $M_\infty < 1$.

We remark that a more pleasing boundary treatment would result if the governing equation, Eq. (8), could be differenced directly on the boundary surface using inward, one-sided, spatial-difference operators. However, the use of one-sided spatial differencing is usually a destabilizing process for diffusion terms, as well as for convection terms whose Jacobian matrices have real eigenvalues of the wrong sign. Consequently, in the present boundary condition treatment, the simple time-independent-like relations of tangency, extrapolation, and, for pressure, Eq. (11), were imposed and applied as described earlier.

IV. Grid Systems

The flow equations have been written in a generalized curvilinear coordinate system that can handle arbitrary surface geometry, including steady and unsteady body motions. The only restriction is due to the thin-layer approximation where it is required that the thin-layer coordinate be ζ, where ζ equals a constant taken as the body surface. Simple body motions such as plunge, rotation, and translation can be handled with linear transformations. More complicated motions and distortions of the grid and body can be introduced as necessary. In our current three-dimensional applications, only steady problems have been solved in which the body and grid system remain stationary.

Because of limited storage capacity on current computers, only simple bodies and geometries have been used. Figure 2 shows the two-grid systems that are used—a warped cylindrical and a warped spherical coordinate. In each case, the grid unfolds into a rectangular computational domain with the body projected onto the lower face. Note that both systems have a coordinate singularity (S in Fig. 2) which is unavoidable in mapping a closed three-dimensional body surface. The singular line is equivalent to either the $r = 0$ line of a cylinder or the polar singularity of a sphere; and, while its location is arbitrary, it is placed here at the nose of the bodies.

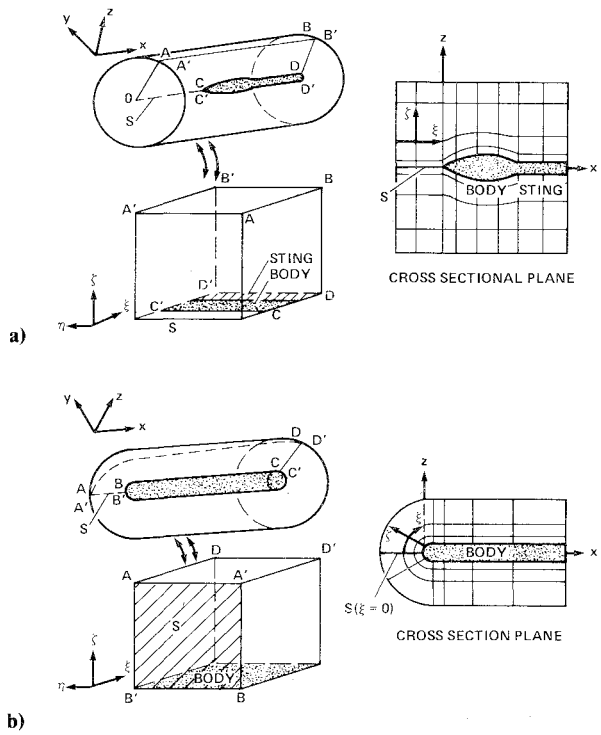

Fig. 2 Coordinate systems: a) warped cylindrical coordinate; b) warped spherical coordinate.

The warped cylindrical coordinate (Fig. 2a) has the disadvantage that, as grid lines are clustered near the body for accuracy and viscous resolution, grid points also cluster toward the singular axis. Points are thus wasted in upstream regions where changes in the flow gradients are small; whereas in the warped spherical system (Fig. 2b), grid lines clustered to the body do not accumulate toward the singular pole. Furthermore, radial grid lines diverge away from the singularity, providing a more efficient distribution of points in the far field.

While a limiting form of the equations would be needed at the singular line, the choice of cylindrical coordinates in inviscid flow or spherical coordinates in inviscid or thin-layer flow allows us to avoid the singularity altogether in the finite-difference formulation. This is because, in either case, $\hat{E}$ and $\hat{G}$ are identically zero on the singular line, even for a time-deforming grid. (Note that $\xi_x/J = (y_\eta z_\zeta - y_\zeta z_\eta)$ and that η derivatives of x,y,z are zero because x,y,z do not change as we rotate around the axis. Likewise, ξ_y/J, ξ_z/J, ξ_x/J, etc., are zero; consequently, from Eq. (2), $\hat{E}$ and $\hat{G}$ are zero.)

Results will be shown for both coordinate systems. Simple shear grids are used about either ogive cylinders or blunted bodies. Exponential clustering is used in the radial-like direction to keep grid points reasonably clustered near the body. For more complex shapes automatic grid generation procedures (see, e.g., Refs. 25-28) can be used which will also produce smoothly varying grids.

V. Results

Solutions have been obtained about isolated body configurations, either ogive sting or a hemisphere cylinder, at various Mach numbers and angles of attack. A typical inviscid

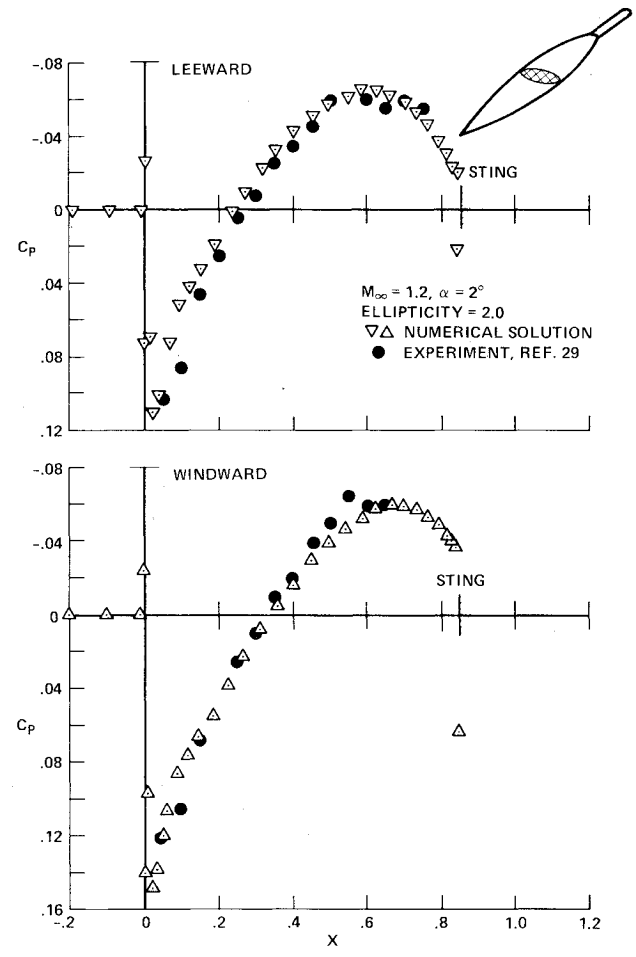

Fig. 3 Parabolic arc body with elliptic cross section at $M_\infty = 1.2$ and $\alpha = 2$ deg.

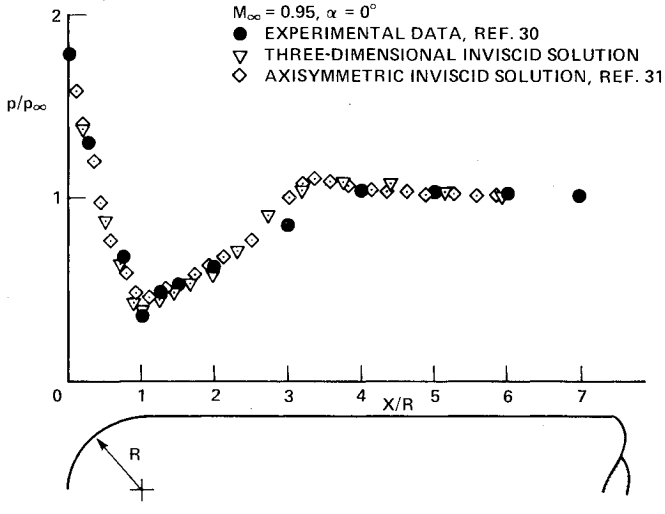

Fig. 4 Transonic flow about hemisphere cylinder, $\alpha = 0$ deg, $M_\infty = 0.95$.

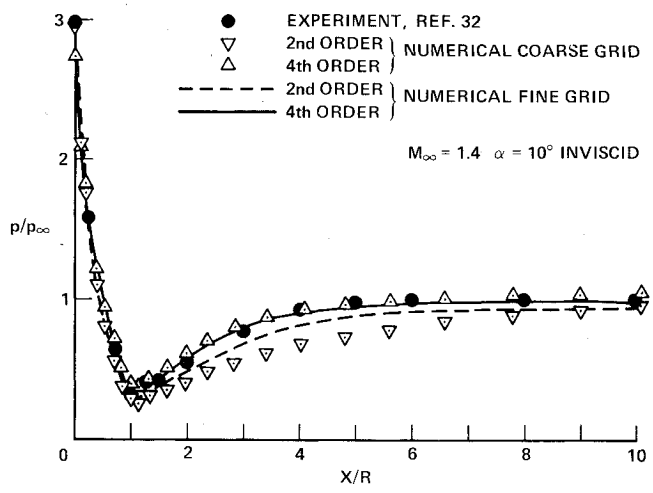

Fig. 5 Hemisphere cylinder, $M_\infty = 1.4$, $\alpha = 10$ deg.

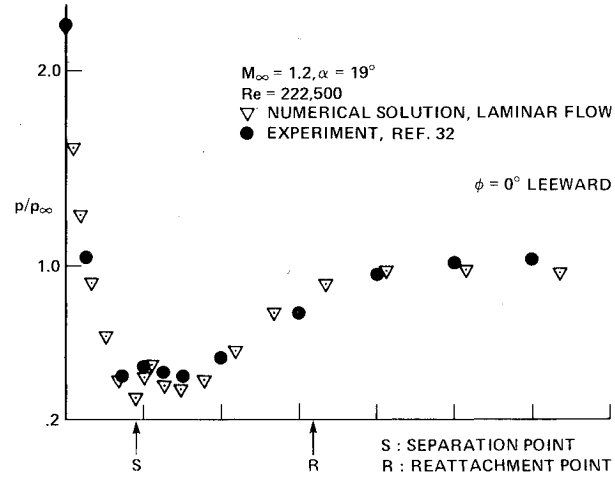

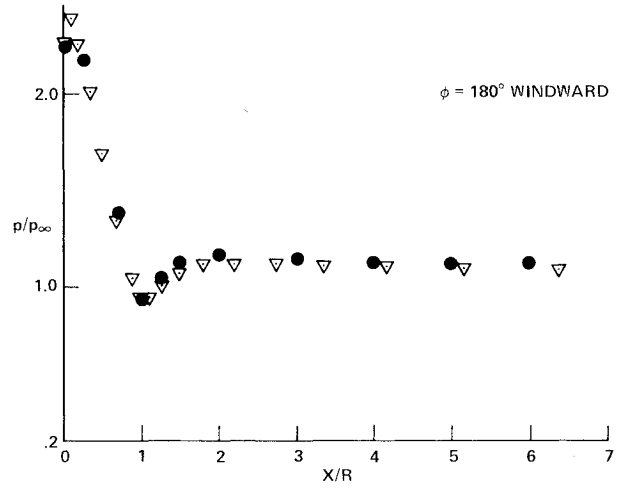

Fig. 6 Hemisphere cylinder at $M_\infty = 1.2$ and $\alpha = 19$ deg.

cylindrical grid consists of 48 points along the body axis—20 points radially, and 12 points in the circumferential direction. A restriction of bilateral symmetry is imposed solely to reduce the computational domain and is not a limitation of the algorithm. The spherical grid usually consists of 30 points along the axis, 30 points in the radial direction, and 12-18 circumferential points with bilateral symmetry imposed. All viscous results were obtained on the hemisphere cylinder at moderate angles of attack so that crossflow asymmetries do not invalidate the bilateral symmetry assumption. For the viscous grids, exponential stretching are used to cluster points near the body.

For freestream Mach numbers close to one, an inviscid steady-state solution is typically obtained in approximately 1 h of CPU time on a Control Data Corporation 7600, while 2-3 h of CPU time are needed for viscous cases. Note that while implicit methods usually imply that large time steps can be taken, it does not automatically follow that fast convergence

to a steady state is achieved. Techniques to improve the algorithm as a viable relaxation procedure are currently being investigated.

A. Inviscid Flow about Ogive Cylinder

Inviscid flow results for an elliptical cross-sectional body at $M_\infty = 1.2$ and $\alpha = 4$ deg are shown in Fig. 3 and are compared with experimental data of McDevitt and Taylor.[29] The numerical and experimental results agree quite well, except for numerical oscillations at the nose that result from the shock-capturing process. Additional inviscid flow results over pointed nose elliptical and circular cross-sectional bodies are given in Ref. 24, which show similar good agreement with experiment.

B. Hemisphere-Cylinder Results

Verification of Accuracy in Inviscid Flow

Switching now to the hemisphere-cylinder cases, a zero angle of attack inviscid solution at $M_\infty = 0.95$ is presented in Fig. 4. Comparisons are made with the experimental results of Hsieh[30] and a numerical calculation by Chaussee using his two-dimensional inviscid axisymmetric code.[31] Both numerical solutions use second-order accurate differencing and are in excellent agreement. Agreement with the experiment is also quite good.

A comparison between solutions using second- and fourth-order spatial differences for the convection terms is shown in Fig. 5 for the leeward side of the hemisphere cylinder at $M_\infty = 1.4$ and $\alpha = 10$ deg. The numerical solutions are also compared with the experimental results of Hsieh.[32] The second-order coarse grid results are inaccurate. Although refining the grid improves the results, they are still somewhat unsatisfactory; better results are obtained when fourth-order differences are used on the coarse grid, and excellent agreement is achieved for fourth-order differences on the fine grid.

The results in Fig. 5 represent extremes of the calculations. It has been our experience that adequate resolution can be obtained for simple body shapes and small angles of attack by means of second-order differencing. However, for more complicated bodies, fourth-order differencing will probably be needed to obtain good accuracy. The addition of fourth-order accuracy (as previously described for steady-state problems) does not substantially increase the computation time.

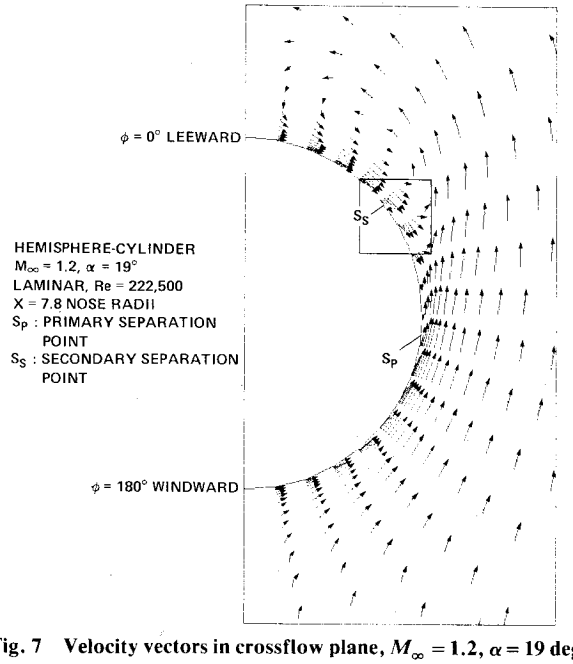

Fig. 7 Velocity vectors in crossflow plane, $M_\infty = 1.2$, $\alpha = 19$ deg.

Viscous Separated Flow at High Incidence and $M_\infty > 1$

A laminar viscous-flow calculation is presented in Fig. 6 for a hemisphere cylinder at $M_\infty = 1.2$ and $\alpha = 19$ deg. Experimental pressure profiles from Hsieh[32] are compared with the numerical calculations obtained using fourth-order accurate differencing. On the leeward side, streamwise separation occurs at the nose which was also reported by Hsieh.[33] Points of streamwise separation and reattachment predicted by the numerical calculation are denoted by S and R in Fig. 6. The boundary layer remains attached on the windward side and numerical results for the windward side are also shown in Fig. 6.

The thin-layer model is capable of predicting the leeside crossflow separation which occurs at this high incidence as well as the preceding predicted streamwise separation. Crossflow velocity vectors from the numerical calculation are shown in Fig. 7 at a downstream station of approximately eight nose radii. Notice the existence of a major recirculation region on the leeside of the cylinder and also a secondary separation region which is seen more clearly in Fig. 8. The calculated crossflow separation lines are shown in Fig. 9 and are compared with the experimental data taken from oil flow pictures.[33] The calculated primary separation line reproduces the experimental data in the region between $X/R = 4$ and $X/R = 8$. Past this point, the combined effects of coarse-grid resolution and the use of the supersonic-outflow boundary

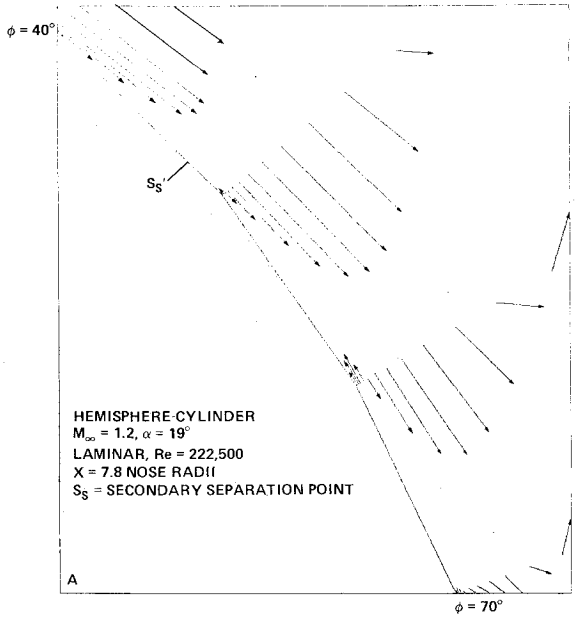

Fig. 8 Velocity vectors in crossflow plane, $M_\infty = 1.2$, $\alpha = 19$ deg.

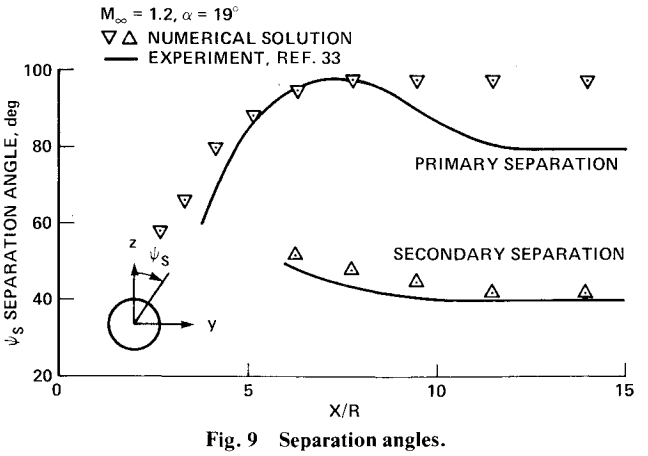

Fig. 9 Separation angles.

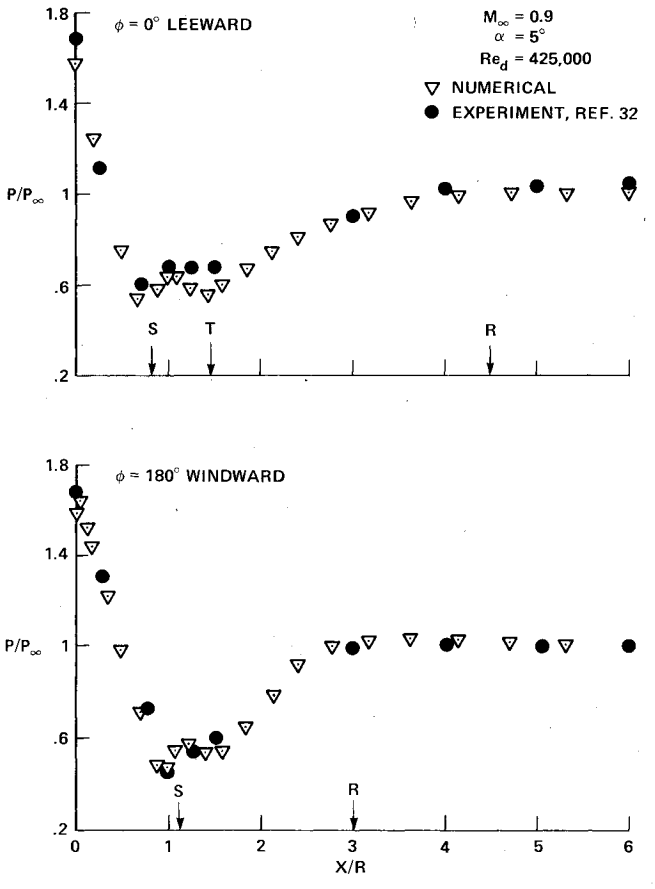

Fig. 10 Transition calculation on hemisphere cylinder.

condition destroy the accuracy of the calculation. The computed secondary separation line is also compared with experimental data in Fig. 9.

Viscous Separated Flow at Moderate Incidence and $M_\infty < 1$

Hsieh[33] also carried out an experiment on a hemisphere cylinder at 5 deg angle of attack in a subsonic freestream, $M_\infty = 0.9$ and $Re_D = 425{,}000$. Numerical laminar and fully turbulent results for this case were presented previously,[24] but were not satisfactory. Leeside streamwise separation was reported by Hsieh[33] and although the laminar numerical results correctly reproduce this feature, a possibly spurious unsteady motion of the flow also occurred. In the numerical turbulence calculation, the results lacked streamwise separation altogether and closely resembled the inviscid results.

Hsieh reports in a private communication that the flow is probably laminar through separation and then transitions to turbulence. To simulate this flow, a transition-turbulence model has been implemented in the thin-layer equations.

To simulate transition, the Baldwin-Lomax[34] algebraic turbulence model was modified so that the eddy viscosity coefficient is set equal to zero until a specified maximum value of eddy viscosity is reached. Downstream of this point, the usual turbulent eddy-viscosity coefficient of the Baldwin-Lomax model is used. For airfoils, Baldwin and Lomax[34] suggest a characteristic constant for transition of 14 in attached boundary layers; whereas in separated regions, a value of 500 is more appropriate.

Numerical results (using fourth-order differencing) obtained with the transition model are shown in Fig. 10 and compared with data from Hsieh.[32] For the windward side, a small area of streamwise flow separation occurs, as reported in the experiment, and the results are in good agreement with the experiment. On the leeward side, separation occurs as in the experiment and a steady flow is obtained which agrees quite well with the experimental pressures. Transition (T) occurs at approximately $X/R = 1.5$ on the leeside and does not occur at all on the windward side of the body. Note that the slight recompression, which occurs after separation in Fig. 10 (also shown in Fig. 6), is due to the rapid growth of the boundary layer after separation. It should be pointed out that these results are rather qualitative and no attempt has been made, at this time, to investigate the finer details of the flowfield.

VI. Conclusions

A general purpose, implicit, finite-difference computer program has been developed to solve compressible unsteady inviscid or thin-layer viscous three-dimensional flow. Applied to current computers, the numerical procedure is capable of providing reasonably accurate flow simulation to simple aerodynamic configurations. Solutions of such airplane-like components can be interesting in their own right and can be useful in testing turbulence models as well. In conjunction with automatic generation of highly warped spherical grids being developed simultaneously with the flowfield solver, simulation of flow about complex aerodynamic configurations can progress when more powerful computers become available.

References

[1] Peyret, R. and Viviand, H., "Computation of Viscous Compressible Flows Based on the Navier-Stokes Equations," AGARD-AG-212, 1975.

[2] Lapidus, A., "A Detached Shock Calculation by Second-Order Finite Differences," *Journal of Computational Physics*, Vol. 2, 1967, pp. 154-177.

[3] Viviand, H., "Conservative Forms of Gas Dynamic Equations," *La Recherche Aerospatiale*, No. 1, Jan.-Feb. 1974, pp. 65-68.

[4] Vinokur, M., "Conservation Equations of Gas Dynamics in Curvilinear Coordinate Systems," *Journal of Computational Physics*, Vol. 14, Feb. 1974, pp. 105-125.

[5] Lindemuth, I. and Killeen, J., "Alternating Direction Implicit Techniques for Two-Dimensional Magnetohydrodynamic Calculations," *Journal of Computational Physics*, Vol. 13, 1973, pp. 181-208.

[6] Briley, W. F. and McDonald, E., "An Implicit Numerical Method for the Multi-Dimensional Compressible Navier-Stokes Equations," Rept. M911363-6, United Aircraft Research Laboratories, 1973.

[7] Beam, R. and Warming, R. F., "An Implicit Finite-Difference Algorithm for Hyperbolic Systems in Conservation-Law-Form," *Journal of Computational Physics*, Vol. 22, Sept. 1976, pp. 87-110.

[8] Beam, R. and Warming, R. F., "An Implicit Factored Scheme for the Compressible Navier-Stokes Equations," AIAA Paper 77-645, June 1977.

[9] "Proceedings of NASA Workshop on Future Computer Requirements for Computational Aerodynamics at the Ames Research Center," Moffett Field, Calif., Oct. 4-6, NASA CP, 2032, 19.

[10] MacCormack, R. W. and Paullay, A. J., "The Influence of the Computational Mesh on Accuracy for Initial Value Problems with Discontinuous or Nonunique Solutions," *Computers and Fluids*, Vol. 2, 1974, pp. 339-361.

[11] Rizzi, A., "Transonic Solutions of the Euler Equations by the Finite Volume Method," in *Proceedings of Symposium Transsonicum II*, K. Oswatitsch and D. Rues, eds., Springer-Verlag, 1976, pp. 567-574.

[12] Deiwert, G. S., "Numerical Simulation of High Reynolds Number Transonic Flows," *AIAA Journal*, Vol. 13, Oct. 1975, pp. 1354-1359.

[13] Steger, J. L., "Implicit Finite Difference Simulation of Flow About Arbitrary Geometries with Applications to Airfoils," AIAA Paper 77-665, 1977.

[14] Lerat, A. and Sides, J., "Numerical Calculation of Unsteady Transonic Flows," Paper presented at AGARD Meeting of Unsteady Airloads in Separated and Transonic Flow, Lisbon, April 1977.

[15] Kutler, P., Chakravarthy, S. R., and Lombard, C. K., "Supersonic Flow Over Ablated Nosetips Using an Unsteady Implicit Numerical Procedure," AIAA Paper 78-213, 1978.

[16] Korn, G. and Korn, T., *Mathematical Handbook for Scientists and Engineers*, McGraw-Hill Book Co., Inc., New York, 1961.

[17] Cheng, H. K., Chen, S. Y., Mobley, R., and Huber, C. R., "The Viscous Hypersonic Slender-Body Problem: A Numerical Approach Based on a System of Composite Equations," The Rand Corp., Santa Monica, Calif., RM 6193-PR, May 1970.

[18] Rubin, S. G. and Lin, T. C., "Numerical Methods for Two- and Three-Dimensional Viscous Flow Problems: Application to Hypersonic Leading Edge Equations," PIBAL Rept. 71-8 (AFOSR-TR-71-0778), 1971.

[19] Lubard, S. C. and Helliwell, W. S., "Calculation of the Flow on a Cone at High Angle of Attack," *AIAA Journal*, Vol. 12, July 1974, pp. 965-974.

[20] McDonald, H. and Briley, W. R., "Three-Dimensional Supersonic Flow of a Viscous or Inviscid Gas," *Journal of Computational Physics*, Vol. 19, 1975, pp. 150-178.

[21] Davis, R. T., "Numerical Solution of the Hypersonic Viscous Shock-Layer Equations," *AIAA Journal*, Vol. 8, May 1970, pp. 843-851.

[22] Warming, R. F. and Beam, R., "On the Construction and Application of Implicit Factored Schemes for Conservation Laws," *SIAM-AMS Proceedings of the Symposium on Computational Fluid Mechanics*, Vol. 11, New York, 1977.

[23] Steger, J. L. and Kutler, P., "Implicit Finite-Difference Procedures for the Computation of Vortex Waves," *AIAA Journal*, Vol. 15, April 1977, pp.

[24] Pulliam, T. H. and Steger, J. L., "On Implicit Finite-Difference Simulations of Three-Dimensional Flow," AIAA Paper 78-10, 1978.

[25] Chu, W. H., "Development of a General Finite Difference Approximation for a General Domain," *Journal of Computational Physics*, Vol. 8, 1971, pp. 392-408.

[26] Thompson, J. F., Thames, F. C., and Mastin, C. M., "Automatic Numerical Generation of Body-Fitted Curvilinear Coordinate System for Fields Containing any Number of Arbitrary Two-Dimensional Bodies," *Journal of Computational Physics*, Vol. 15, 1974, pp. 299-319.

[27] Thames, F. C., Thompson, J. F., and Mastin, C. M., "Numerical Solution of the Navier-Stokes Equations for Arbitrary Two-Dimensional Airfoils," NASA SP-347, Pt. I, March 1975, pp. 469-530.

[28] Ghia, U. and Ghia, K. N., "Numerical Generation of a System of Curvilinear Coordinates for Turbine Cascade Flow Analysis," University of Cincinnati Rept. No. AFL 75-4-17, 1975.

[29] McDevitt, J. B. and Taylor, R. A., "Force and Pressure Measurements at Transonic Speeds for Several Bodies Having Elliptical Cross Sections," NACA TN 4362, 1958.

[30] Hsieh, T., "Low Supersonic, Three-Dimensional Flow About a Hemisphere-Cylinder," AIAA Paper 75-836, June 1975.

[31] Chaussee, D., "On the Transonic Flow Field Surrounding Tangent Ogive Bodies with Emphasis on Nose Drag Calculation," AIAA Paper 78-212, 1978.

[32] Hsieh, T., "An Investigation of Separated Flow About a Hemisphere-Cylinder at 0- to 90-deg Incidence in the Mach Number Range from 0.6 to 1.5," AEDC-TR-76-112, July 1976.

[33] Hsieh, T., "An Investigation of Separated Flows About a Hemisphere-Cylinder at Incidence in the Mach Number Range from 0.6 to 1.5," AIAA Paper 77-179, Jan. 1977.

[34] Baldwin, B. S. and Lomax, H., "Thin Layer Approximation and Algebraic Model for Separated Turbulent Flows," AIAA Paper 78-257, 1978.